

Article

Tracking Robot Location for Non-Destructive Evaluation of Double-Shell Tanks

Christopher Cree ¹, Emily Carter ¹, Heng Wang ², Changki Mo ¹ and John Miller ^{1,*}

¹ Washington State University Tri-Cities, School of Engineering and Applied Sciences, Richland, WA 99354, USA; christopher.cree@wsu.edu (C.C.); emily.barkley@wsu.edu (E.C.); changki.mo@wsu.edu (C.M.)

² Pacific Northwest National Laboratory, Richland, WA 99354, USA; dangwh@hotmail.com

* Correspondence: jhmiller@tricity.wsu.edu

Received: 30 August 2020; Accepted: 13 October 2020; Published: 19 October 2020



Featured Application: Robotic inspections of double-shell nuclear-waste storage tanks at the Department of Energy's Hanford site.

Abstract: (1) Background: Non-destructive evaluation of double-shell nuclear-waste storage tanks at the U.S. Department of Energy's Hanford site requires a robot to navigate a network of air slots in the confined space between primary and secondary tanks. Situational awareness, data collection, and data interpretation require continuous tracking of the robot's location. (2) Methods: Robot location is continuously monitored using video image analysis for short distances and laser ranging for absolute location. (3) Results: The technique was demonstrated in our laboratory using a mockup of air slot and robot. (4) Conclusions: Location tracking and display provide decision support to inspectors and lay the groundwork for automated data collection.

Keywords: computer vision; image analysis; laser ranging

1. Introduction

Double-shell tanks (DSTs) are a critical part of the infrastructure at the U.S. Department of Energy's Hanford site, where a large volume of defense-related nuclear waste is being managed and processed toward ultimate storage in an immobilized state. Hanford DSTs have been used for interim storage of partially liquid nuclear waste since their construction in years 1971–1986. They are expected to continue to serve this function until 2050, which is the target date for completion of the immobilization process for all Hanford nuclear waste. If this target is reached, DSTs will have been used 14–15 years beyond their original projected lifetime [1]. Consequently, for the next approximately 30 years, the integrity of Hanford DSTs for storage of nuclear waste will need to be monitored.

Under the direction of the U.S. Department of Energy's Office of River Protection (DOE-ORP), the Pacific Northwest National Laboratory (PNNL) has partnered with Hanford Tank Operations contractor Washington River Protection Solutions (WRPS) to develop a robotic non-destructive evaluation (NDE) technology for DSTs. The NDE process is expected to have two phases. The first phase will use a low-resolution electromagnetic acoustic transducer (EMAT) sensor [2,3] developed by the Southwest Research Institute [4] to scan large regions of the primary tank bottom. These scans will be used to prioritize air slots, designed for cooling, for deployment of a robot-driven high-resolution guided wave phased array (GWPA) sensor [5] developed by Guidedwave [6,7].

Continuous monitoring of the robot's position as it navigates the narrow air slots in the confined space between primary and secondary tanks is critical for the decision support to operators and will ultimately allow robot control to be automated. It is also necessary for interpretation of the high-resolution ultrasonic data from multiple locations. Knowing these locations with a precision of

± 0.5 inches allows a map to be constructed of regions of interest for repeated inspection. Methods under development to track robot location with this precision include sound-wave reflections, length of cable laid out to the robot, and the optical methods discussed in this paper.

Due to poor illumination of the air slot, location tracking by video analysis is limited to relative measurements of short distances. Absolute location obtained by chaining these short movements together can lead to a large accumulation of error. Laser ranging does not suffer from these limitations but may fail due to motion of the robot that moves the laser off target. Videos can detect these failures and initiate tracking by image analysis based on the last valid laser-ranging data. The return of the laser to the target resets the absolute location. This combination of optical techniques was investigated in a laboratory mockup of air slot and robot.

2. Materials and Methods

To facilitate the use of robot-location tracking for decision support, a graphical user interface (GUI) for NDE operations was written in the .NET framework using the Visual Studio integrated development environment based on the Windows Presentation Foundation and C# as the programming language. XAML is used as the GUI designer and Model-View-Viewmodel is used as the display pattern. The GUI displays video footage from cameras on the robot traveling in the air slots and real-time data from the ultrasonic sensor at the selected measurement sites. A composite image constructed from ultrasonic sensor data collected at multiple sites can replace the real-time data if desired.

The GUI moves a marker on a map of air slots to illustrate the location of the robot during data collection. This display also shows tank-specific weld patterns connecting plates that make up the bottom of the primary tank in spatial relation to air slots in the refractory concrete pad under the primary tank. Data to construct the overlay of welds and air slots were kindly provided by WRPS staff. The pattern of welds in the bottom of the primary tank varies for tanks constructed at different times. We used data provided by WRPS to generate overlays for AZ-, SY- and AW-type DSTs. AN- and AP-type DSTs have the same tank-bottom weld pattern as AW-type DSTs. All these DST types have the same air-slot pattern in the refractory pad.

Image analysis to enhance the information content of video footage from the cameras on the robot was carried out in the Scientific Python Development Environment, Spyder 4.0.1, using cv2, a computer vision software package that includes OpenCV Canny Edge Detection [8]. Initial analysis was conducted on a 15-min video from visual inspection of air slot 31-1 in DST tank AP-107 [9] and kindly provided to us by WRPS staff. Additional video footage was obtained, and the results of the analysis were tested in our laboratory at WSU-TC using an air-slot mockup kindly provided to WSU by PNNL.

Data were obtained with a vehicle pulled manually through the mockup while carrying a small laser range finder and two cameras recording forward and rear videos. The U81 laser range finder (JRT Meter Technology) was chosen for its small size ($17 \times 41 \times 7$ mm), weight (4 g), and voltage requirements (2.5–3.3 V). The VoCam264 (ameriDroid) was chosen for its small size ($20 \times 20 \times 25$ mm) and to achieve 30 fps at resolution 1920×1080 . The entrance to the channel was covered with graph paper with 5-mm squares, on which a horizontal line was drawn 30 mm long and at the height of the camera in the robot mockup. This line was used to determine the effective F -value to use in the triangle-similarity method [10] to determine the distance of the camera from an object. The length of the line in pixels was measured in an image with the camera a known distance from the entrance of the channel as measured by the laser range finder.

Pulling the robot mockup down the channel using cables coming from the camera and laser induced roll into the motion. The extent of roll was reduced by a cable management system but could not be eliminated. Since tilting the robot toward either side of the channel changes the perspective of the image relative to that of the calibration set up, we collected the data necessary to implement the triangle-similarity method in the presence of roll. To accomplish this, we lined the channel with 5-mm-square graph paper, being careful that the grid was parallel and perpendicular to the top edge

of the channel. We highlighted four grid points—two on each side of the channel 50 mm apart—at the top of the channel, and recorded video footage with the robot mockup tilted to the left- and right-side of the channel.

Figure 1 shows a conceptual drawing of a robot to move sensors through the air slots under DSTs for NDEs. Our mockup of this design has only one unit with cable attachments that allowed us to manually pull the unit through the air-slot mockup in our lab with the camera pointing toward the entrance. A 3D-printed camera holder was mounted on top of the unit with the laser range finder mounted directly below the rear camera.

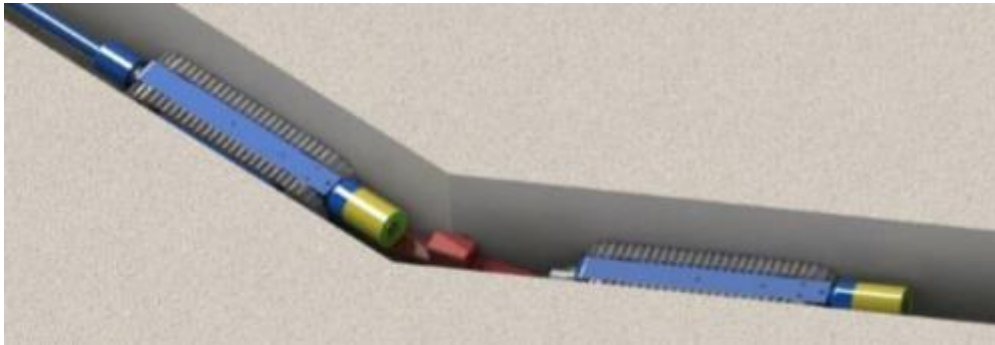


Figure 1. Conceptual design of a robot to move sensors through air slots. Three-unit design allows the robot to navigate bends. Cameras on crawler units are shown in yellow. The red unit between crawlers carries sensor and actuator. Reprinted from [11] with permission.

3. Results

Figure 2 shows a screen shot of the graphical user interface (GUI) developed to display the position of the robot in an air slot. Air slots are bifurcated structures shown by the blue lines in the diagram on the left-hand side of Figure 2. The red lines show the AP-type tank-bottom weld pattern in relation to air slots.

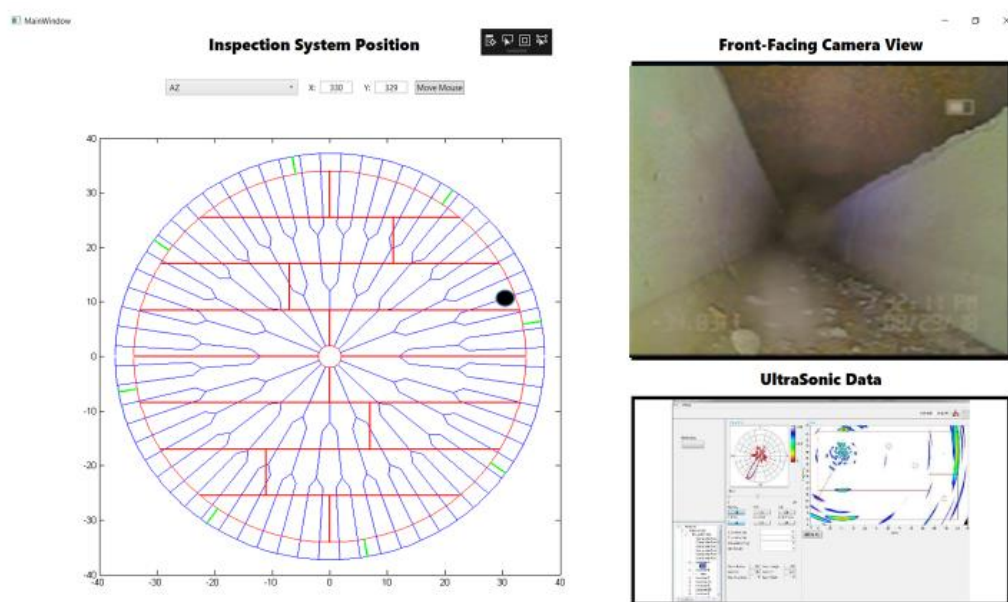


Figure 2. Graphical User Interface to display the robot position in the air slot (left), a video frame from a camera on the robot (top right), and data like that expected from non-destructive evaluation (NDE) of double-shell tanks (DSTs) (bottom right). The black dot indicates the position of the robot in the air slot.

Tank AP-107 has 24-inch annulus-access risers labeled 030 and 031 at the 90- and 270-degree positions, respectively, in the air-slot diagram on the left-hand side of Figure 2. The black dot on the air slot near annulus-access riser 030 shows how tracking of the robot's location in an air slot will be dynamically displayed on the GUI. The top-right panel in Figure 2 is the part of the GUI reserved for real-time display of video footage from a camera on the robot. In Figure 2, this function is illustrated by a video frame from visual inspection of air slots in tank AP-107 [6]. The image shown in the bottom-right panel of Figure 2 illustrates various types of data that can be transmitted from the robot to inspection personnel. This portion of the GUI will most often be used to display real-time data from the GWPA sensor and messages to the operator.

Several methods of position tracking are currently under investigation, including cable layout and ultrasonic reflections. We have focused on laser ranging augmented by video analysis. Due to poor illumination in the air slot, video analysis is not practical as a stand-alone system because absolute location of the robot must be the accumulation of many relative measurements of motion toward markers in the region currently illuminated by light sources on the robot. Such a method is vulnerable to large error due to the accumulation of error in relative distances.

Laser ranging is not limited by illumination of the air slot but may fail if movement of the robot carrying the laser causes it to bounce off the walls of the air slot rather than the end of the channel that is a known distance from the entrance. Video analysis complements laser ranging in this situation because the spot illuminated by the laser pointer is present in the video, which can be used to monitor misalignment leading to faulty readings. When this happens, video analysis takes over location tracking using the last accurate report from laser ranging as the absolute location of the robot. Restoration of proper alignment, which can be seen in the video, signals return to tracking by laser ranging.

Triangle similarity [10] is the most common approach to distance measurement in image analysis. It requires calibration of the camera, which can be performed offline, to determine the apparent focal length $F = PD/W$, where D is the distance to an object of known width W , and P is the width of the image of the object in pixels. Given F , we can calculate distance $D = WF/P$ to any mark of known width W from its image width in pixels. If P_1 and P_2 are image widths of the mark in earlier and later frames, respectively, then the robot has moved a distance $WF/P_1 - WF/P_2$ toward the mark in the time between those frames. In our laboratory experiments, we use a rear camera pointed toward the channel entrance. In this arrangement, the distance moved away from a mark is $WF/P_2 - WF/P_1$.

The main challenge in using triangle-similarity for tracking is that the motions that move the laser spot off its target and create a need for video analysis complicate its implementation because the perspective of the image is no longer the same as the perspective used in calibration. To a first approximation, we can allow for the change in perspective by calculating P_1 and P_2 in a model that corresponds to the analytical geometry of the perspective used in calibration. In this analytical geometry, the triangle formed by the intersection of the lines in the image—defined by the top edges of the air slot and the line of length P connecting points opposite each other across the top of the air slot—is isosceles. To test this model, we performed experiments in our lab with a vehicle carrying two cameras and the laser range finder, moved manually down the air-slot mockup provided by PNNL.

A video frame taken from the rear camera in our experiments is shown in Figure 3. The channel has been carefully lined with graph paper so that points directly opposite each other on the top edge could be easily identified. Figure 3 shows four of these points connected by lines. The lengths of these lines in pixels, determined from the frame coordinates shown in Table 1, are 311 and 570 pixels for far and near lines, respectively. Using these results for P_1 and P_2 in the formula $WF/P_1 - WF/P_2$ with $W = 73.9$ mm, the measured width of the channel at its top, and $F = 452$ pixels, the experimentally determined focal length of the rear camera, triangle similarity predicts the lines are separated by 48.8 mm. This result differs from the expected 50 mm derived from marks on the graph paper by only 1.2 mm.

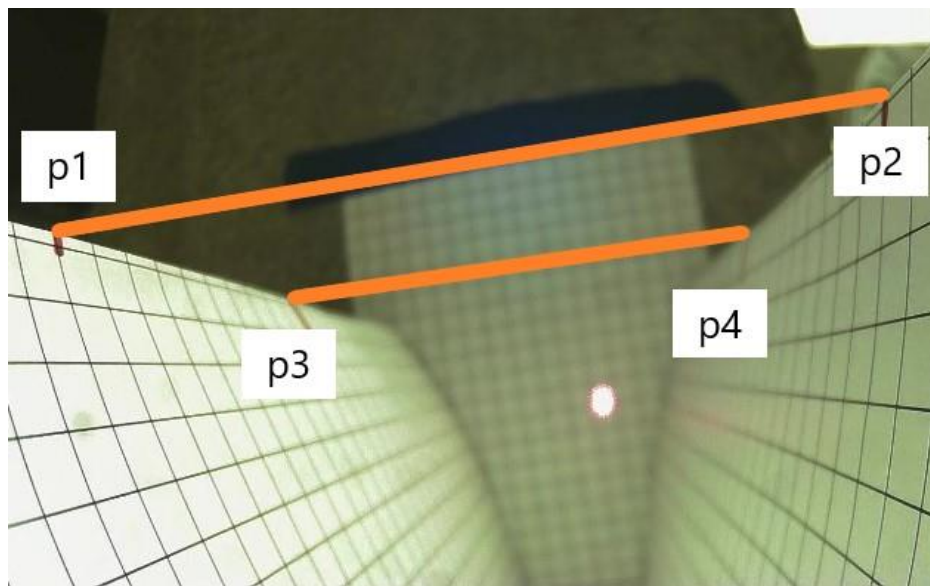


Figure 3. View from rear camera showing graph-paper lined channel marked with points 50 mm apart on the top edges. Spot where laser hits graph paper covering channel entrance shows that the vehicle is tilted toward the right-hand wall of the channel.

Table 1. Coordinates of line end points in Figure 3.

	x	y
p1	537	841
p2	1099	748
p3	697	885
p4	1005	842

The approach used in the laboratory to find P_1 and P_2 will not be available for analysis of the video footage taken in the air slots because the point that is directly opposite the target on the other side of the air slot will not be known. Edge-detection in video analysis can be used to determine the slopes of the intersections of an air slot with the tank bottom. Given these slopes and the coordinates of a feature in the air-slot–tank-bottom interface, the isosceles-triangle model can predict the width of the air slot in pixels at the targeted feature. We tested this approach on the images obtained in our laboratory experiments with the vehicle tilted left and right by comparison with the lengths of near and far lines, like those shown in Figure 3, calculated from the coordinates of their endpoints. Errors in the predictions of the isosceles-triangle model in 24 cases ranged between 3% and 18% of the true values. These results motivated us to develop a linear regression model of corrections to the isosceles-triangle model. Optimum slope and y-intercept obtained with a training set of 24 examples are 0.349055 and -0.220441 , respectively. Predictions of the corrected model on six new cases that are midway between the near and far training examples are shown in Table 2.

Table 2. Performance of corrected isosceles-triangle model on a test set of experimental data.

Left Edge Slope	% Difference from Actual Width Using Isosceles Method	% Difference after Correction
0.618892508	3.605%	−4.047%
0.980263158	9.758%	2.415%
0.291066282	−9.825%	−2.059%
0.605166052	−1.622%	0.701%
0.952380952	10.781%	0.418%
0.282786885	−15.158%	2.985%

The results in Table 2 show that we have sufficient accuracy in calculations of the apparent width of the top of the channel in pixels to use this width for tracking the movement of the robot toward a selected feature in the interface of the air slot with the tank bottom. Estimates of the uncertainty in the method were obtained by repeated application of video analysis using the vertical grid lines in Figure 3 as targets for the apparent change in channel width as the robot moved away from the target. Results are shown in Table 3. Mean and standard deviation of absolute error are 1.466 ± 1.033 mm.

Table 3. Repeated application of the corrected isosceles-triangle model for distance measurements.

Model Estimate (mm)	Graph-Paper Standard (mm)	Difference (mm)
17.038	20	-2.962
40.267	40	0.267
31.655	30	1.655
23.31	25	-1.69
35.756	35	0.756

To demonstrate this method under conditions similar to those in air slots, we covered the air-slot mockup in our laboratory and selected a feature in the interface between the channel and cover as a marker to track the movement of our vehicle a short distance down the channel. Figure 4 shows that the laser is hitting the cover on the entrance to the channel to provide a measurement of distance traveled down the channel that can be compared with the results of the image analysis. Video analysis predicts the robot has moved 68.63 mm and laser ranging measurements show that the robot has moved 67 mm.

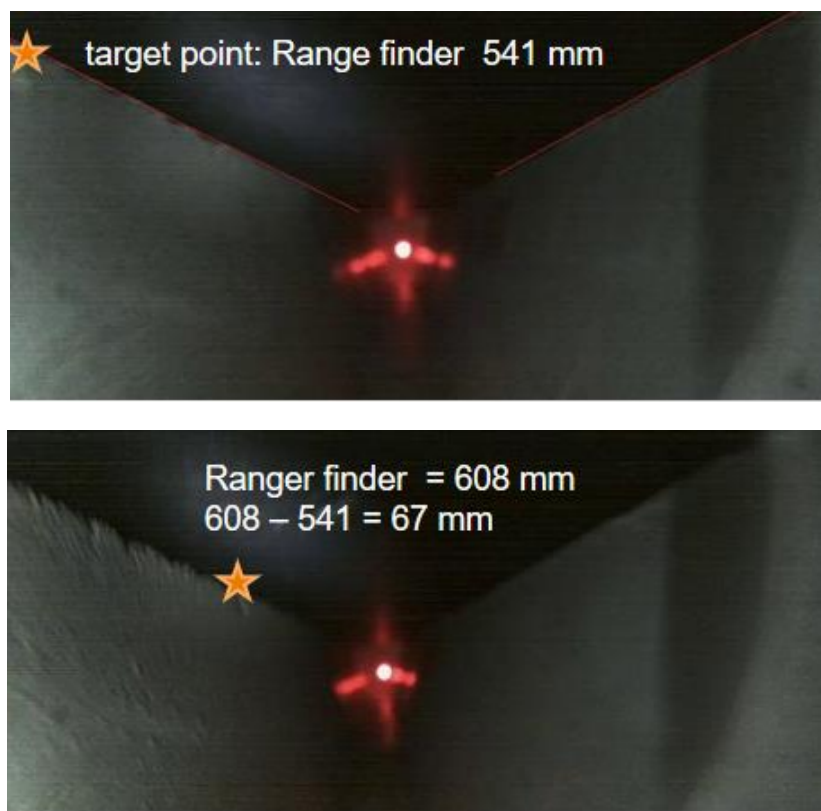


Figure 4. In the top panel, the target is selected, and calculated to be 40.99 mm from camera. In the bottom panel, the robot has moved away from the target and is calculated to be 109.63 mm from the camera.

4. Discussion

Currently, inspection of DSTs at the Hanford site by a high-resolution ultrasonic sensor is labor intensive. Operators control robot movement while watching multiple computer screens displaying data in different formats. We have developed a GUI that brings some of these data into one display with multiple windows. A large portion of the display contains a map of air slots in relation to tank-bottom welds on which the location of the robot can be dynamically displayed. This alerts the operator to turns in the channel that should be confirmed by the video feed. It also shows the approach of the robot to tank-bottom welds that will have a major effect on the data from the ultrasonic sensor when welds are close to a data collection site. The location of data collection sites needs to be known with a precision of approximately one inch to enable the development of a composite image from data collected at multiple sites.

Our research has focused on optical methods to track the robot's location in an air slot. A laser range finder that meets the requirements of size, weight, power consumption, etc., to be part of the robot assembly is the centerpiece of our design. Since the tractors that move the ultrasonic sensor in and out of the air slot have no guidance mechanism, off-center and misalignment can move the range finder away from its target. When this happens, a backup location-tracking system is needed until centering and alignment are restored, possibly by operator intervention. We have demonstrated that the analysis of video footage acquired at the same time as laser-range-finder output can serve this purpose. Since the U81 laser range finder has a laser pointer, video analysis can automate the switch from laser to video and back. This is the immediate goal of our ongoing research in the lab. A somewhat more distant goal is to automate the selection and tracking of a feature in the video to be the basis for the triangle-similarity approach to location tracking. Edge detection is expected to be key to this development.

Author Contributions: Conceptualization, C.M., J.M., C.C. and E.C.; methodology, C.C. and E.C.; software, H.W. and C.C.; validation, C.M., E.C. and C.C.; formal analysis, J.M. and C.C.; investigation, C.C. and E.C.; resources and funding, C.M.; writing—original draft preparation, J.M.; writing—review and editing, J.M., C.C., E.C. and C.M. All authors have read and agreed to the published version of the manuscript.

Funding: This research was funded by the Pacific Northwest National Laboratory, grant number 516084.

Acknowledgments: The authors gratefully acknowledge assistance from Washington River Protection Solutions staff members who provided data on the structure of Hanford DSTs that enabled us to map the air-slot network in relation to tank-bottom welds and the Pacific Northwest National Laboratory for the realistic air-slot mockup provided to WSU-TC. This mockup enabled demonstration of the validity and effectiveness of our proposed position-tracking techniques.

Conflicts of Interest: The authors declare no conflict of interest. The funders had no role in the design of the study; in the collection, analyses, or interpretation of data; in the writing of the manuscript, or in the decision to publish the results.

References

1. Girardot, C.; Venetz, T.; Boomer, K.; Johnson, J. Hanford Single-Shell Tank and Double-Shell Tank Integrity Programs. In Proceedings of the Waste Management Symposium, Phoenix, AZ, USA, 6–10 March 2016; p. 16390.
2. Ludwid, R.; You, Z.; Palanisamy, R. Numerical simulations of an electromagnetic acoustic transducer-receiver system for NDT applications. *IEEE Trans. Magn.* **1993**, *29*, 2081–2089. [[CrossRef](#)]
3. Ribichini, R.; Cegla, F.; Nagy, P.B.; Cawley, P. Experimental and numerical evaluation of electromagnetic acoustic transducer performance on steel materials. *NDT E. Int.* **2012**, *45*, 32–38.
4. Denslow, K.; Glass, S.; Larche, M.; Boomer, K.; Gunter, J. Hanford Under-tank Inspection with Ultrasonic Volumetric Non-destructive Examination Technology. In Proceedings of the Waste Management Symposium, Phoenix, AZ, USA, 18–22 March 2018; p. 18470.
5. Zhoa, J.; Durham, N.; Abdel-Hati, K.; McKenzie, C.; Thomson, D.J. Acoustic guided wave techniques for detecting corrosion damage of electric grounding rods. *Measurement* **2019**, *147*, 106858. [[CrossRef](#)]

6. Borigo, C.; Love, R.; Owens, S.; Rose, J.L. Guided Wave Phased Array Technology for Rapid Inspection of Hanford Double Shell Tank Liners. In Proceedings of the ASNT Annual Conference, Nashville, TN, USA, 30 October–2 November 2017.
7. Denslow, K.; Moran, T.; Larche, M.; Glass, S.; Boomer, K.; Kelly, S.; Wooley, T.; Gunter, J.; Rice, J.; Stewart, D.; et al. Progress on Advancing Robotic Ultrasonic Volumetric Inspection Technology for Hanford Under-tank Inspection. In Proceedings of the WM2019 Conference, Phoenix, AZ, USA, 3–7 March 2019; p. 19474.
8. Bradski, G. The OpenCV Library. *Dr. Dobb J. Softw. Tools* **2000**, *120*, 122–125.
9. Gunter, J.R. Primary Tank Bottom Visual Inspection System Development, and Initial Deployment at Tank AP-107. RPP-RPT-61208. November 2018.
10. Rosebrock, A. Triangle Similarity for Object/Marker to Camera Distance. Available online: <https://www.pyimagesearch.com/2015/01/19/find-distance-camera-objectmarker-using-python-opencv/1/19/2015> (accessed on 1 June 2020).
11. Dobell, C.; Robinson, S. Marsupial Miniature Robotic Crawler System for Camera and Sensor Deployment in Nuclear Waste Double Shell Tank Refractory Air Slots. In Proceedings of the ASNT Annual Conference, Nashville, TN, USA, 30 October–2 November 2017.

Publisher's Note: MDPI stays neutral with regard to jurisdictional claims in published maps and institutional affiliations.



© 2020 by the authors. Licensee MDPI, Basel, Switzerland. This article is an open access article distributed under the terms and conditions of the Creative Commons Attribution (CC BY) license (<http://creativecommons.org/licenses/by/4.0/>).